Published online 29 April 2020

Nucleic Acids Research, 2020, Vol. 48, No. 11 ***6149–6156***
doi: 10.1093/nar/gkaa298

Fuse to defuse: a self-limiting ribonuclease-ring nuclease fusion for type III CRISPR defence

Aleksei Samolygo[1,2,†], Januka S. Athukoralage[2,†], Shirley Graham[2] and Malcolm F. White[2,*]

[1]Skolkovo Institute of Science and Technology, Bolshoy Boulevard, 30/1, Moscow 121205, Russian Federation and [2]Biomedical Sciences Research Complex, School of Biology, University of St Andrews, North Haugh, St Andrews, Fife KY16 9ST, UK

Received March 11, 2020; Revised April 13, 2020; Editorial Decision April 14, 2020; Accepted April 17, 2020

ABSTRACT

Type III CRISPR systems synthesise cyclic oligoadenylate (cOA) second messengers in response to viral infection of bacteria and archaea, potentiating an immune response by binding and activating ancillary effector nucleases such as Csx1. As these effectors are not specific for invading nucleic acids, a prolonged activation can result in cell dormancy or death. Some archaeal species encode a specialised ring nuclease enzyme (Crn1) to degrade cyclic tetra-adenylate (cA_4) and deactivate the ancillary nucleases. Some archaeal viruses and bacteriophage encode a potent ring nuclease anti-CRISPR, AcrIII-1, to rapidly degrade cA_4 and neutralise immunity. Homologues of this enzyme (named Crn2) exist in type III CRISPR systems but are uncharacterised. Here we describe an unusual fusion between cA_4-activated CRISPR ribonuclease (Csx1) and a cA_4-degrading ring nuclease (Crn2) from *Marinitoga piezophila*. The protein has two binding sites that compete for the cA_4 ligand, a canonical cA_4-activated ribonuclease activity in the Csx1 domain and a potent cA_4 ring nuclease activity in the C-terminal Crn2 domain. The cA_4 binding affinities and activities of the two constituent enzymes in the fusion protein may have evolved to ensure a robust but time-limited cOA-activated ribonuclease activity that is finely tuned to cA_4 levels as a second messenger of infection.

INTRODUCTION

Type III CRISPR systems have class 1 effector complexes that utilize CRISPR RNA (crRNA) to detect RNA from mobile genetic elements (MGE) such as viruses. This target RNA binding results in the activation of the Cas10 subunit, which commonly harbours two active sites: an HD nuclease domain for ssDNA cleavage (1–3) and a PALM polymerase domain that cyclises ATP to generate cyclic oligoadenylate (cOA) molecules (4–7). cOA acts as a second messenger in the cell, signalling infection and activating a range of auxiliary defence enzymes such as the ribonuclease Csx1/Csm6 (8–10) or the DNA nickase Can1 (11) by binding to a CRISPR-associated Rossman fold (CARF) sensing domain. Once activated, these enzymes degrade both host and invading nucleic acids in the cell, which can result in viral clearance (i.e. immunity) or lead to cell dormancy or even death (akin to Abortive Infection) (12). Detection of 1 viral RNA by the *Sulfolobus solfataricus* type III-D CRISPR system can lead to the generation of 1000 molecules of cyclic tetra-adenylate (cA_4), equivalent to an intracellular concentration of 6 μM cA_4, which is sufficient to fully activate the Csx1 ribonuclease (13).

The potency and high amplification factor inherent in type III cA_4 signalling necessitates a mechanism to clear cA_4 from the cell—otherwise cells could be driven to 'commit suicide' unnecessarily. In *S. solfataricus*, cells express a specialised catalytic variant of a CARF-domain protein named 'CRISPR-associated ring nuclease 1' (Crn1) that binds and slowly degrades cA_4, returning cells to a basal, uninfected state (14). The CARF domains of some members of the Csm6 family have also been shown to have ring nuclease activity, slowly degrading cA_4 and thus acting as self-limiting ribonucleases (9,15). More recently, a potent ring nuclease enzyme of viral origin has been identified that acts as an anti-CRISPR (Acr) by rapidly degrading cA_4 to circumvent type III CRISPR immunity (16). The enzyme, AcrIII-1, is a small dimeric protein unrelated to the CARF domain that uses an active site histidine residue to ensure higher catalytic efficiency (16). Biochemical and modelling studies have revealed that AcrIII-1, which is widespread in archaeal viruses and bacteriophage, efficiently deactivates Csx1 *in vitro* (17).

Homologues of AcrIII-1 are also found in association with type III CRISPR systems in some genomes, where they

*To whom correspondence should be addressed. Tel: +44 1334 463432; Fax: +44 1334462595; Email: mfw2@st-andrews.ac.uk
†The authors wish it to be known that, in their opinion, the first two authors should be regarded as Joint First Authors.

have been predicted to function in the host defence against MGE. In this context, the enzyme has been named Crn2 (CRISPR-associated ring nuclease 2) (16). We previously noted an unusual (so far, unique) example of a Crn2 gene fused to a Csx1 ribonuclease in the type III CRISPR locus of the organism *Marinitoga piezophila* (16), and herewith we term this gene product Csx1–Crn2 (Figure 1). The *M. piezophila* CRISPR locus includes a type III-B effector, an RNA-guided Argonaute enzyme (18) and an uncharacterised CARF-RelE protein that may be activated by cOA to cleave ribosomal A-site mRNA (19). Sequence analysis suggests that Csx1–Crn2 consists of a canonical Csx1 protein, including an N-terminal CARF domain for cOA sensing and HEPN (Higher Eukaryotes, nucleotide sensing) ribonuclease domain, fused to a Crn2 domain at the C-terminus (Figure 1B; Supplementary Figure S1). The 563 aa protein is predicted to form a dimer as dimerization is fundamental to the structure and function of both constituent domains, and a structural model generated by Swissmodel (17) using the templates Csx1 (PDB 6R7B) and AcrIII-1 (PDB 6SCF) is shown in Figure 1C.

Here, we express, purify and characterise the Csx1–Crn2 protein, revealing cA_4-activated ribonuclease activity associated with the Csx1 domain and a potent cA_4 ring nuclease activity catalysed by the Crn2 domain – the first cellular ring nuclease of this family to be studied. Biochemical analysis of the wild-type and engineered variant forms of the enzyme allow the mechanism of this self-limiting antiviral defence enzyme to be delineated.

MATERIALS AND METHODS

Cloning and expression

For cloning, a synthetic gene (g-block) encoding the Csx1–Crn2 protein, codon optimised for *Eschericia coli*, was purchased from Integrated DNA Technologies (IDT), Coralville, USA, and cloned into the vector pV5HisTev (20) between the NcoI and BamHI sites. Competent DH5α cells were transformed with the construct and sequence integrity confirmed by sequencing (Eurofins Genomics). A single conservative mutation (V177L) in a variable region of the protein was noted in the cloned gene but was not deemed problematical. The plasmid was transformed into *E. coli* C43 (DE3) cells for protein expression. Two liters of LB culture was grown at 37°C to an OD_{600} of 0.3 with shaking at 180 rpm. Protein expression was induced with 0.4 mM Isopropyl β-D-1-thiogalactopyranoside and cells were grown at 37°C overnight before harvesting by centrifugation at 4000 rpm (Beckman Coulter Avanti JXN-26; JLA8.1 rotor) at 10°C for 10 min.

Protein purification

Expression and purification of *Sulfolobus islandicus* rod-shaped virus 1 gp29 (AcrIII-1) has been described previously (16). For Csx1-Crn2 purification, the cell pellet was resuspended in four volumes equivalent of lysis buffer containing 50 mM Tris–HCl 7.5, 0.5 M NaCl, 10 mM imidazole and 10% glycerol supplemented with EDTA-free protease inhibitor tablets (Roche; 1 tablet per 100 ml buffer) and lysozyme (1 mg/ml). Cells were lysed by sonication (six times 1 min with 1 min rest intervals on ice) and the lysate was centrifuged at 40 000 rpm (70 Ti rotor) at 4°C for 30 min. The lysate was filtered (0.45 μm) and then loaded onto a 5 ml HisTrap FF Crude column (GE Healthcare) equilibrated with wash buffer containing 50 mM Tris–HCl pH 7.5, 0.5 M NaCl, 30 mM imidazole and 10% glycerol. Unbound protein was washed away with 20 column volumes (CV) of wash buffer prior to elution of his-tagged protein using a linear gradient (holding at 10% for 3 CV, and 50% for 3 CV) of elution buffer containing 50 mM Tris–HCl pH 7.5, 0.5 M NaCl, 0.5 M imidazole and 10% glycerol. SDS-PAGE was carried out to identify fractions containing the protein of interest, and relevant fractions were pooled and concentrated using a 30 kDa molecular weight cut-off centrifugal concentrator (Merck). The his-tag was removed by incubating concentrated protein overnight with Tobacco Etch Virus (TEV) protease (1 mg per 10 mg protein) while dialyzing in buffer containing 50 mM Tris–HCl pH 7.5, 0.5 M NaCl, 30 mM imidazole and 10% glycerol at room temperature. The protein with his-tag removed was filtered (0.45 μm) and isolated using a 5 ml HisTrapFF column, eluting the protein using 4 CV wash buffer. Cleaved protein was filtered (0.45 μm) and further purified by size-exclusion chromatography (Superdex S200 26/60; GE Healthcare) in buffer containing 20 mM Tris pH 7.5, 0.25 M NaCl using an isocratic gradient. After SDS-PAGE, fractions containing protein of interest were concentrated and protein was aliquoted and stored at −80°C.

Variant enzymes were generated using the QuickChange Site-Directed Mutagenesis kit as per manufacturer's instructions (Agilent technologies), verified by DNA sequencing and purified as for the wild-type protein.

RNase assays

The RNA oligonucleotide A1 was purchased from IDT and RNA labeling was carried out as described previously (4). For RNA degradation assays, 50 nM radiolabelled RNA A1 was incubated with Csx1-Crn2 (5 or 10 μM dimer) with 100 μM of cyclic oligoadenylate (cA_3, cA_4 or cA_6) in Reaction buffer (20 mM MES pH 6.5, 150 mM NaCl, 1 mM EDTA, 1 mM DTT and 0.06 U/μl SUPERase•In RNase Inhibitor) for 30 min (or other indicated timepoints), at 50°C. Reactions were quenched by adding phenol–chloroform–isoamyl alcohol (Ambion) and vortexing. For single-turnover RNA cleavage kinetics experiments, a mix of 50 nM radiolabelled RNA A1 and 100 μM cA_4 was prepared in pH 6.5 reaction buffer as above and pre-warmed at 50°C for 5 min. Addition of pre-warmed enzyme (10 μM dimer Csx1–Crn2 or its variants) started the reaction. At indicated times, 10 μl of the reaction was taken and quenched by adding to phenol–chloroform and vortexing. Subsequently, the deproteinised RNA cleavage products were mixed (1:1) with 100% formamide xylene–cyanol loading dye and separated by denaturing polyacrylamide gel electrophoresis (PAGE; 20% acrylamide, 7 M urea, 1× TBE, 45°C, 3000 V) for 2 h. Following the electrophoresis, the gels were phosphorimaged at −70°C overnight. For RNA kinetic analysis, substrate RNA and degradation products were quantified using the Bio-Formats plugin of ImageJ as distributed in the

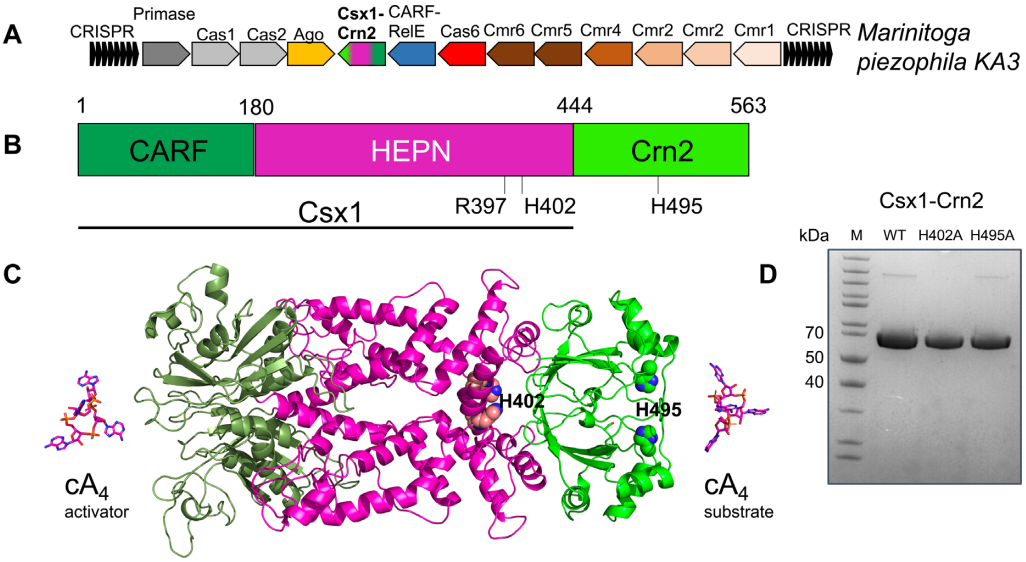

Figure 1. The atypical type III CRISPR system of M. piezophila. (**A**) CRISPR locus of *M. piezophila* (NCBI accession NC_016751) includes genes encoding a complete type III-B (Cmr1–6, Cas6) gene cluster, adaptation proteins Cas1 and Cas2, argonaute, and two uncharacterised CARF-domain proteins: CARF-RelE and Csx1-Crn2. (**B**) Cartoon of the Csx1-Crn2 protein highlighting the N-terminal Csx1 ribonuclease and C-terminal Crn2 ring nuclease components. (**C**) Structural model of Csx1–Crn2. The active site residues of the HEPN ribonuclease (R397, H402) and ring nuclease (H495) are shown in spheres. Domain colouring is as for part B. Although the structures of the Csx1 and Crn2 domains are predicted with high confidence, their relative orientation is not known and the model shown here represents just one possible conformation. (**D**) SDS-PAGE analysis of purified recombinant Csx1Crn2 wild-type and variants.

Fiji package and a background signal was subtracted as described previously (20). Fraction cleaved was calculated for every time point and fitted via GraphPad Prism 8 to an exponential graph $Y = Y0 + (\text{Plateau} - Y0) *(1 - \exp(-K*x))$ with $Y0$ fixed to 0 (one phase association).

A1 oligo: 5′-AGGGUAUUAUUUGUUUGUUUCU UCUAAACUAUAAGCUAGUUCUGGAGA

cA_4 pre-incubation assay

Prior to the addition of RNA, 10 μM enzyme dimer WT or its variant H495A were mixed with 10, 50 or 100 μM cA_4 in reaction buffer and incubated for 10 min at 50°C. To start the reaction, ∼50 nM radiolabelled RNA A1 was added and the reactions were incubated for a further 30 min at the same temperature before quenching and analysis as described above.

cA_4 degradation assays

Radiolabelled cyclic oligoadenylates were generated enzymatically using type III-D effector complex of *S. solfataricus*, as described previously (14). For cA_4 cleavage assay, ∼200 nM radiolabeled cA_4 was incubated with either 1 or 5 μM dimer Csx1–Crn2 or its variants in reaction buffer at 50°C, over a set of time points as indicated in the relevant figure legends. As a positive control, cA_4 and 1 μM AcrIII-1 SIRV1 gp29 were assayed for 1 min. At the desired time points, 10 μl of the reaction was removed and quenched by adding to phenol–chloroform and vortexing. Deproteinised products were then further isolated by chloroform-isoamyl alcohol extraction (Sigma-Aldrich) for thin-layer chromatography. As a negative control, cA_4 was incubated to the end-point of each experiment.

Multiple-turnover kinetics

For multiple turnover kinetics of cA_4 cleavage, a reaction mix composed of 256 μM unlabelled cA_4, ∼100 nM radiolabelled cA_4 and varying concentration of enzyme dimer (160, 320, 480, 640, 1280, 2560 and 5120 nM) in Reaction buffer was prepared and incubated at 50°C. Addition of pre-warmed enzyme to the reaction mix started the reaction. At certain time points, 10 μl of the reaction was removed, quenched, and extracted as described above. RNA cleavage was then visualised by denaturing PAGE and the fraction of RNA cut was quantified and initial rates were calculated. Initial rates were plotted against substrate concentration and fitted to a linear equation on GraphPad Prism 8 to obtain the multiple-turnover rate of cA_4 cleavage by Csx1–Crn2.

Thin-layer chromatography (TLC)

TLC was carried out as described previously (16). In brief, a glass chamber was pre-warmed for 1 h at 38°C and then left to humidify with 0.5 cm of TLC buffer (100 ml; 0.2 M ammonium bicarbonate pH 9.2, 70% ethanol, H_2O) for a further 45 min. 1 μl of sample was spotted 1 cm from the bottom of a 20 cm × 20 cm silica gel on TLC Aluminium foil plate (Supelco Sigma-Aldrich) and the TLC plate was placed into the humidified glass chamber, sealed, and the buffer was allowed to migrate up the plate for ∼3 h at 35°C (until the migration front reached ∼17 cm). The TLC plate was then air dried and phosphorimaged overnight.

Electrophoretic mobility shift assay

For the binding assay, 10 nM radioactively-labelled cA_4 was incubated with Csx1–Crn2 variants H495A, H129W and

S452Y at varying concentrations in binding buffer containing 20 mM Tris–HCl pH 7.5, 150 mM NaCl and 2 mM $MgCl_2$ supplemented with 2 μM Ultrapure Bovine Serum Albumin (Invitrogen) for 10 min at 25°C. Following the incubation, samples were mixed with an equivalent volume of 20% (v/v) glycerol and equal volumes were run on a native polyacrylamide gel (15% acrylamide, 1× TBE) at 250 V, 30 W and 28°C for ∼3 h. Binding was visualized by phosphorimaging at −70°C overnight.

RESULTS

Expression and purification of Csx1–Crn2

A synthetic gene (g-block) encoding the *M. piezophila* Csx1–Crn2 protein, codon optimised for expression in *Escherichia coli*, was cloned into the pEV5hisTev plasmid (20), allowing expression of the recombinant protein with a cleavable N-terminal polyhistidine tag. The protein was purified to near homogeneity by a combination of immobilized metal affinity and size exclusion chromatography (Figure 1D). Enzyme variants with mutations targeted to the active site of the Csx1 ribonuclease (H402A) or the Crn2 enzyme (H495A) were expressed and purified as for the wild-type enzyme.

The N-terminal domain of Csx1-Crn2 is a cA_4-activated ribonuclease

Type III CRISPR systems typically synthesize a range of cOA molecules with a ring size varying from 3–6 (4–7,21). We first wished to determine the identity of the activator for Csx1–Crn2 by incubating the enzyme with an RNA substrate (RNA A1) in the presence of cA_3, cA_4 or cA_6. Only cA_4 activated the ribonuclease activity of the enzyme (Figure 2A), consistent with the predicted structural similarity to the cA_4-activated Csx1 protein of *S. islandicus* (10). A variant enzyme with a mutation targeted to the HEPN ribonuclease active site (H402A) was inactive for RNA degradation, but the H495A variant with a mutation targeted to the Crn2 active site appeared more active than the wild-type enzyme (Figure 2B). Overall, these data confirmed that the HEPN domain of Csx1-Crn2 was responsible for RNA cleavage and suggested that the ring nuclease activity might serve to limit the ribonuclease activity.

We noted that the RNA substrate was processed in the absence of cA_4 activator by trimming of a small number of nucleotides from the 3′ end (e.g. Figure 2A lane 2). This activity was abolished in the H495A variant (e.g. Figure 2B lane c1) suggesting that the ring nuclease domain is capable of processing the 3′ ends of RNAs independent of cA_4 activation. This RNase activity is reminiscent of the CARF-family protein Csx3, which has been described as a deadenylase (22) and has parallels with the observed binding of *S. islandicus* Csx1 to the 3′ tetra-adenylate tails of mRNA (23). The 3′-terminus of the RNA A1 substrate consists of four purine nucleotides (GAGA). While cA_3 and cA_6 did not support target RNA degradation, they did block RNA trimming (Figure 2A), suggesting they still compete with RNA for binding to the Crn2 active site.

The C-terminal domain of Csx1–Crn2 is a highly active ring nuclease specific for cA_4 degradation

Having established that cA_4 was the activator of the Csx1 domain, we tested the ability of the Crn2 domain to degrade cA_4 *in vitro* (Figure 3A). Rapid degradation of cA_4 to linear A_2>P (di-adenylate with a 3′-cyclic phosphate) was observed within the first minute of the assay, followed by a slower conversion of A_2>P to A_2-P (di-adenylate with a 3′-phosphate). Overall, the reaction rate and products were highly reminiscent of the AcrIII-1 enzymes studied previously (16). A variant enzyme with a mutation targeted to the predicted active site histidine of the Crn2 domain (H495A) did not degrade cA_4, confirming the Crn2 domain as the site for ring nuclease activity. The single-turnover reaction kinetics of the Csx1–Crn2 ring nuclease activity were too rapid to quantify, suggesting a catalytic rate constant of the order of 10 min^{-1}. To explore this more fully, we carried out a series of kinetic experiments under multiple turnover conditions, using 256 μM cA_4 substrate and varying the concentration of Csx1–Crn2 from 0.16 nM to 5.12 μM (Figure 3B). The initial reaction rate at each enzyme concentration was quantified and plotted, yielding data that could be fitted with a linear fit of slope 8.8 ± 0.3 min^{-1} (Figure 3B). Assuming that the enzyme is saturated at 256 μM cA_4, this affords an estimation of k_{cat} for the ring nuclease activity of about 9 min^{-1}—in good agreement with the single turnover data for Csx1–Crn2 and other related ring nucleases (16). Thus, the Crn2 active site is a highly active ring nuclease capable of rapid, multiple-turnover degradation of the cA_4 activator and does not appear to be significantly rate-limited by substrate binding or product release.

Deactivation of the ring nuclease activity enhances ribonuclease activity of Csx1–Crn2

Having established the activities of the Csx1 and Crn2 domains individually, we next wished to investigate how the two enzymatic domains collaborate to potentiate cA_4-activated RNA degradation. Firstly, we pre-incubated the wild-type or H495A variant forms of the enzyme with cA_4 for 10 min, then added wild-type enzyme together with radiolabelled substrate RNA to assess Csx1 activity (Figure 4A). When the (ring nuclease inactive) H495A variant was used in the pre-incubation, robust RNA degradation by Csx1 was observed at all three cA_4 concentrations tested (Figure 4B). However, following pre-incubation with wild-type Csx1-Crn2, RNA degradation was minimal except for the highest concentration of cA_4 (100 μM). This experiment demonstrated that Csx1–Crn2 can self-deactivate (in bulk terms) by degrading cA_4 in the ring nuclease site.

We next quantified RNA degradation over time in a reaction including 10 μM Csx1–Crn2 (wild-type or H495A variant), 100 μM cA_4 and ∼50 nM radioactively labelled substrate RNA. The wild-type enzyme displayed more rapid initial kinetics, degrading approximately 50% of the RNA within 2 min, but quickly reached a plateau after which RNA was not further degraded (Figure 4C). In contrast, the H495A variant, which is unable to degrade cA_4, had a slower rate constant but completely degraded all the substrate RNA in the course of the 30 min incubation. The slower initial rate may be due to cA_4 sequestration by the

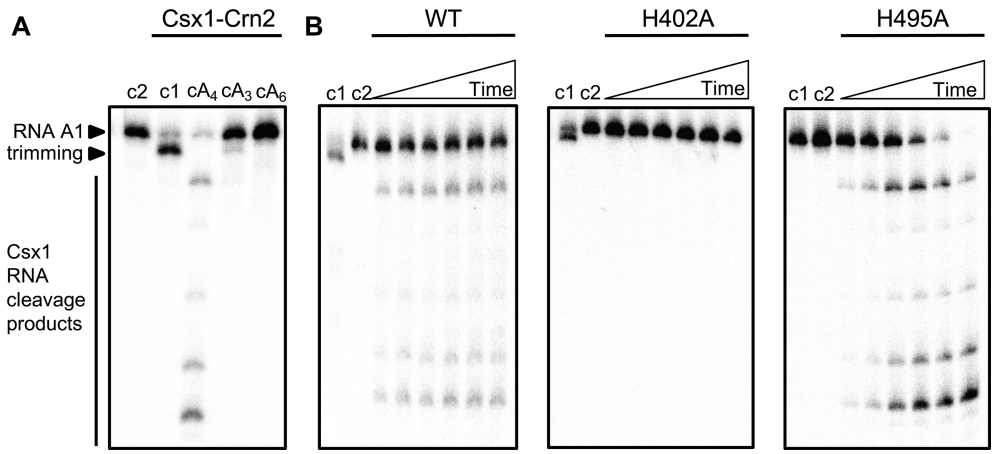

Figure 2. The Csx1 domain of Csx1–Crn2 is a cA_4-activated ribonuclease. (**A**) RNase assay to determine activator of Csx1 domain. Phosphorimage of denaturing PAGE shows the radiolabeled RNA A1 (50 nM) assayed with 1 μM Csx1–Crn2 dimer and a cyclic activator (100 μM): cA_4 (cyclic tetra-adenylate), cA_3 (cyclic tri-adenylate), or cA_6 (cyclic hexa-adenylate). Samples were incubated at 50°C for 30 min. The control lanes c1 and c2 show the assay in the absence of activator or the absence of enzyme, respectively. The data are representative of three technical replicates. (**B**) Phosphorimage of denaturing PAGE visualising degradation of radiolabeled RNA by Csx1-Crn2 or its variant H402A (10 μM dimer) when activated by cA_4 (100 μM) at 50°C (time points are 1, 2, 4, 10, 15, 30 min). Control reactions carried out to the end-point of each assay without cA_4 (c1) or without enzyme (c2) are shown. The data is representive of three technical replicates.

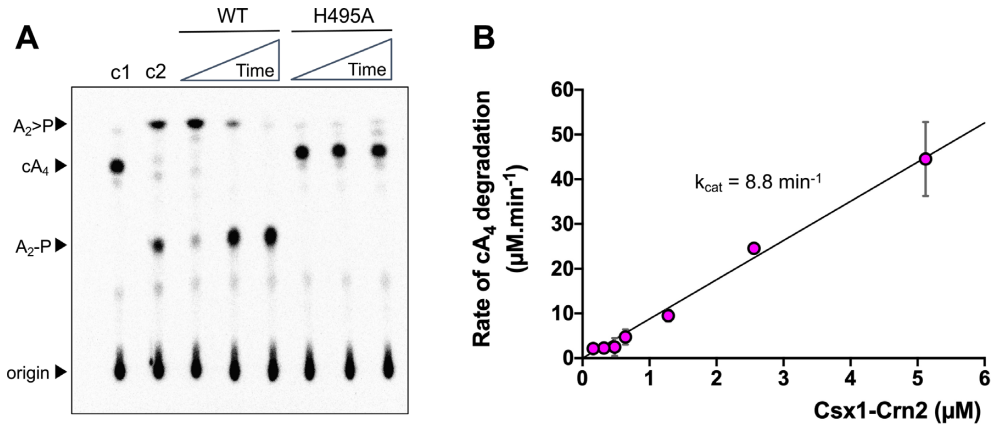

Figure 3. Csx1–Crn2 rapidly degrades cA_4. (**A**) Phosphorimage of thin-layer chromatography (TLC) visualising degradation of radiolabelled cA_4 (~200 nM) by Csx1-Crn2 or its H495A variant (1 μM dimer) at 50°C over time (1, 10, 60 min). Control reactions incubating radiolabelled cA_4 with buffer (c1, negative control) for 60 min or with 1 μM AcrIII-1 for 1 min (c2, positive control) are also shown; the data are representative of three technical replicates. (**B**) Csx1–Crn2 rapidly degrades cA_4 under multiple-turnover conditions. The initial rate of cA_4 (256 μM) degradation was quantified at different concentrations of Csx1–Crn2 protein and plotted. A linear function was fitted through the origin and the catalytic rate constant k_{cat} was estimated ($k_{cat} = 8.8 \pm 0.3\ min^{-1}$). Each data point is the average of at least three technical replicates and error bars show standard deviation of the mean.

Crn2 binding site, but it is also possible that the H495A mutation results in a reduced specific activity of the Csx1 enzyme by unspecified means. Thus, the two active sites have the ability to cooperate to ensure that cA_4-stimulated RNA degradation is regulated, potentially limiting the cellular response to viral infection.

cA_4 binding affinity of the Csx1-CARF and Crn2 domains

Next, we wished to understand the interaction between cA_4 and the CARF and Crn2 domains of Csx1-Crn2 that bind the second messenger. We first investigated cA_4 binding by the H495A variant, which can bind but not cleave cA_4 in the Crn2 site, by electrophoretic mobility shift assay (EMSA), using ~10 nM radioactively-labeled cA_4 (Figure 5B). A clear gel-shift was observed yielding an apparent K_D of around 20 nM, which is similar to that previously observed for stand-alone ring nucleases (13). As there are two cA_4 binding sites in the protein, we next designed variant enzymes to abolish cA_4 binding in either the CARF (H129W) or Crn2 (S452Y) binding sites, guided by the structural model shown (Figure 5A) and multiple sequence alignment (Supplementary Figure S1). These bulky amino acid substitutions were predicted to prevent or significantly reduce cA_4 binding without destabilising the protein structure (Supplementary Figure S2). The two variants were purified as for the wild-type protein, and cA_4 binding was assessed by EMSA (Figure 5B). The S452Y variant showed no obvious binding of cA_4, but cleavage of cA_4 at high protein concentrations (apparent $K_D \sim 1$ μM) suggested that the cA_4 binding at the ring nuclease site was strongly reduced but not abolished. The H129W variant cleaved cA_4 into A_2>P

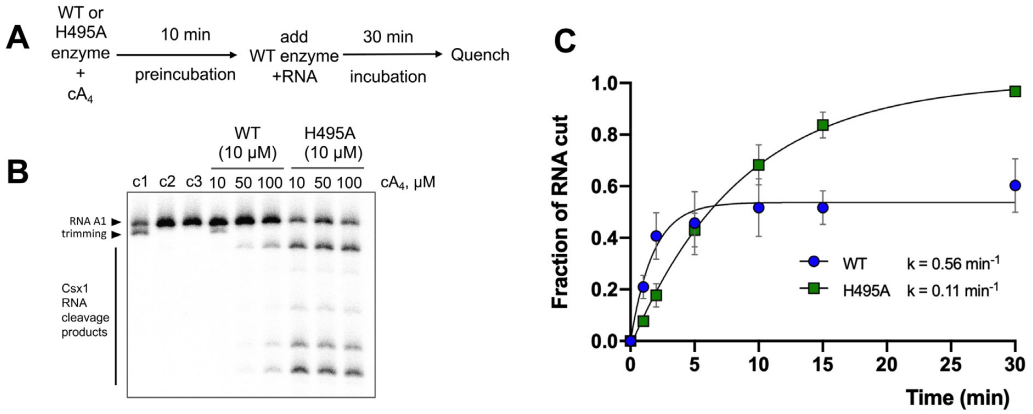

Figure 4. Csx1-Crn2 is an example of a self-limiting ribonuclease. (**A**) The scheme of the pre-incubation experiment. (**B**). Denaturing PAGE shows degradation of radiolabelled RNA (50 nM) by WT or its H495A variant (10 μM dimer) that were pre-incubated with 10, 50 or 100 μM cA_4 at 50°C for 10 min prior to addition of radiolabelled RNA A1, followed by incubation for a further 30 min. A set of control reactions in the same conditions but lacking cA_4 (c1), enzyme (c2) or both (c3) are shown. The data represent the results of three technical replicates. (**C**). Quantification of fraction of RNA degraded by either Csx1-Crn2 (WT) or its H495A variant (10 μM dimer) at 50°C over time. The results were fitted with an exponential equation and estimated rates of RNA cleavage are shown (WT, $k = 0.56 \pm 0.11$ min^{-1}, plateau $= 0.54 \pm 0.03$; H495A, $k = 0.11 \pm 0.01$ min^{-1}, plateau $= 1.02 \pm 0.03$). The data points are the average of three technical replicates and error bars show standard deviation of the mean.

at a concentration of 20 nM enzyme, consistent with high affinity binding and cleavage at the Crn2 site. Overall, these data suggest that the CARF domain has a weaker intrinsic affinity for cA_4 than the ring nuclease domain. Otherwise, we would have expected to see higher affinity binding of cA_4 by the CARF domain of the S452Y variant. However, we cannot rule out the possibility that the S452Y mutation results in weaker binding of cA_4 by the CARF domain.

We also tested the ring nuclease and RNA cleavage activities of the two variant enzymes (Figure 5C, D). As predicted, the S452Y variant had a severely reduced, although not abolished, ring nuclease activity—consistent with the EMSA result. The H129W variant was a fully active ring nuclease, ruling out a model whereby the two cA_4 binding sites communicate to control cA_4 degradation. As expected, the H129W variant had no cA_4-activated RNase activity, confirming that this variant does not bind cA_4 in the CARF domain. Neither of the variants targeting the ring nuclease domain had a discernible effect on the activity of the Csx1 ribonuclease.

DISCUSSION

The importance of cyclic nucleotide signalling in prokaryotic anti-viral defence systems is an emerging paradigm. Examples include cA_4 and cA_6 for type III CRISPR (5,6), cA_3 for the HORMA-DncV-NucC system (24,25) and a variety of cyclic dinucleotides synthesised by diverse CBASS enzymes (26,27). Viruses have a clear imperative to degrade these molecules and circumvent immunity, but it is increasingly apparent that cellular immune systems also need a mechanism to turnover these second messengers if they are to prevent runaway toxicity and cell death (13). For type III CRISPR systems at least, immunity rather than abortive infection may be the *modus operandi*, as mechanisms exist to 'kill the messenger'. Ring nucleases that degrade cA_4 include the dedicated enzymes and self-limiting ribonucleases based on the CARF domain (9,14,15) and the DUF1874 family whose members include the viral anti-CRISPR AcrIII-1 and putative cellular Crn2 proteins (16).

Crn2 ring nucleases have been detected in diverse bacterial genomes associated with type III CRISPR defence but not yet characterised. Here, we focussed on an unusual fusion of a Csx1 ribonuclease and Crn2 ring nuclease from *Marinitoga piezophila*, whose genome also has a CRISPR-associated Argonaute enzyme and an uncharacterised, predicted cA_4-activated RelE toxin (Figure 1). We have demonstrated that the fused protein does indeed combine the activities of a canonical cA_4-activated Csx1 ribonuclease and a highly active ring nuclease. The ring nuclease activity, with a k_{cat} of 9 min^{-1}, is on a par with the highly active viral Acr enzymes (16) and ~20-fold more active than Crn1, suggesting that cellular Crn2 enzymes are not always 'de-tuned' to act more slowly than their viral cousins. The level of ring nuclease activity required in a cell may of course depend on the concentration of cA_4 synthesised by different type III CRISPR systems. Furthermore, the existence of a fusion between Csx1 and Crn2 means that the relative concentrations of the two enzymes can not be varied in response to infection—they are of necessity fixed at 1:1. This is a distinct advantage when exploring the logic of a complex system as the relative concentrations of the effectors are defined with certainty.

These observations raise the intriguing question of how the two activities collaborate to provide appropriate levels of immunity. Our *in vitro* analyses clearly demonstrate that the ring nuclease activity limits, but does not abolish, the cA_4-activated ribonuclease activity of Csx1 (Figure 4). One can rationalise this by assuming that the two enzymes compete for binding of cA_4, and that once activated, the Csx1 enzyme can catalyse multiple rounds of RNA cleavage before the activator dissociates. Only then is there a chance to degrade it at the Crn2 active site. The balance between ribonuclease and ring nuclease enzyme activities will thus largely be determined by their relative affinities for cA_4. Perhaps surprisingly, we observe that the Crn2 domain binds

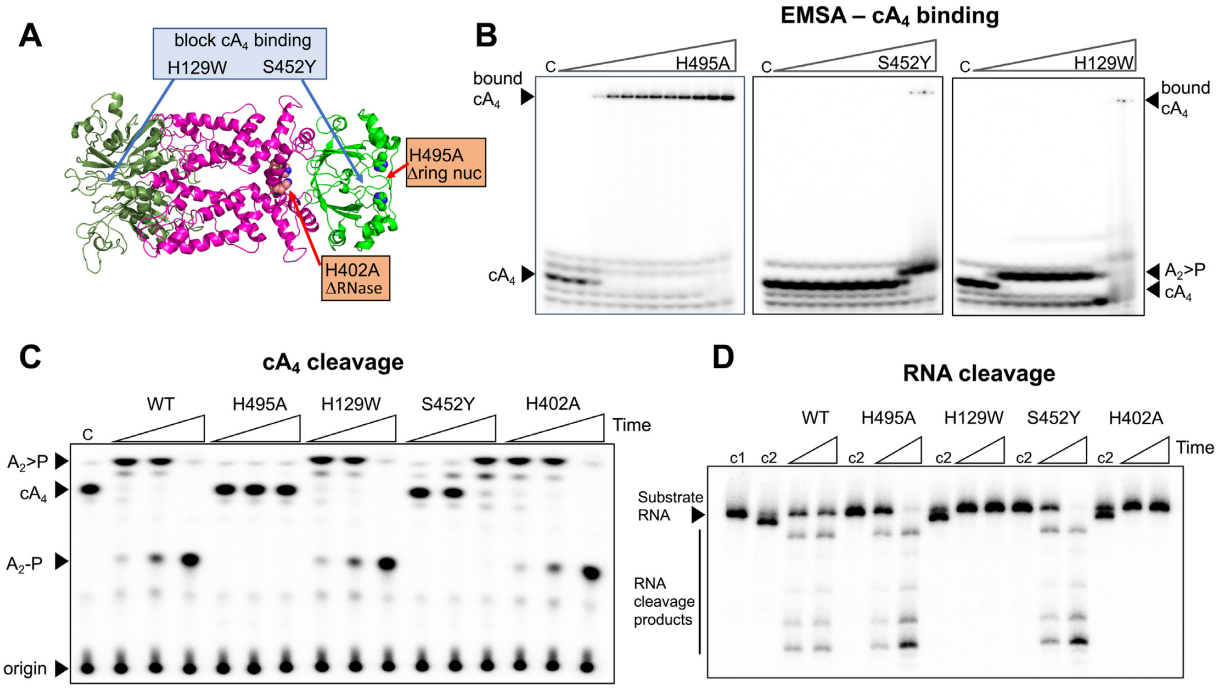

Figure 5. Dissection of cA_4 binding and catalysis by Csx1–Crn2. (**A**) Cartoon representation of Csx1–Crn2 showing sites targeted by mutagenesis. (**B**). Electrophoretic mobility shift assay (EMSA) showing binding of radiolabelled cA_4 (~10 nM) by Csx1-Crn2 variants (0.001, 0.01, 0.02, 0.03, 0.04, 0.05, 0.06, 0.08, 0.1, 1.0, 10.0 and 20.0 μM, respectively). On each gel is a control reaction (c) with cA_4 in the absence of protein. The ring nuclease defective variant H495A bound cA_4 with an apparent dissociation constant around 20 nM. The S452Y variant, which was designed to abolish cA_4 binding by the ring nuclease domain, had a severe binding defect, with cA_4 degradation apparent at high protein concentrations. The H129W variant, designed to abolish cA_4 binding in the CARF domain, showed cA_4 degradation starting from around 20 nM enzyme. The data are representative of three technical replicates. (**C**) TLC showing degradation of cA_4 (200 nM) by wild-type and variant enzymes (5 μM dimer) at 50°C. A time-course of 10 s, 1 min and 10 min was carried out and a control reaction (c) incubating buffer with radiolabeled cA_4 for 10 min is also shown. The H495A variant was inactive as shown previously. The H129W and H402A variants targeting the CARF and HEPN (Csx1) domains, respectively, had normal ring nuclease activity. Whereas the S452Y variant targeting the Crn2 domain had strongly reduced activity, consistent with weaker binding of cA_4 by the Crn2 domain. (**D**) Denaturing PAGE showing cleavage of radiolabelled substrate RNA (100 nM) by Csx1-Crn2 and variants (5 μM dimer) and 100 μM cA_4 at 50°C. RNA cleavage was examined at two time-points (5 & 30 min) and control reactions incubating radiolabelled RNA in buffer (c1) or RNA and protein in the absence of cA_4 activator (c2) for 30 min are also shown. The H129W and H402A variants were inactive as expected. The data are representative of three technical replicates.

cA_4 much more tightly than the CARF domain (apparent K_D ~20 nM and > 1 μM, respectively). This suggests that the RNase activity of Csx1 will only be licensed once cA_4 concentrations reach high μM levels in the cell. This is not necessarily a limitation, as the large degree of signal amplification generated by type III CRISPR systems can result in a 6 μM concentration of cA_4 in cells detecting only 1 viral RNA, generated over 20–30 min (4,13). Indeed, this characteristic could be beneficial in shielding the cell from inappropriate/transient firing of cA_4 production due to self-targetting events, for example. It should also be noted that a second cA_4-activated defence enzyme is encoded by the CRISPR locus of *M. piezophila*—a predicted RelE enzyme that may be licensed by cA_4 binding to cleave mRNA undergoing translation. Thus the Crn2 ring nuclease may need to function in the deactivation of two enzymes that could be toxic to the cell if not restrained. Overall, this study highlights the pressing need for prokaryotic cells to have a mechanism to remove cyclic nucleotide second messengers efficiently in circumstances where abortive immunity is not the desired outcome, or to dampen down any spurious activation of the pathway in the absence of phage infection.

SUPPLEMENTARY DATA

Supplementary Data are available at NAR Online.

ACKNOWLEDGEMENTS

Author contributions: A.S. designed experiments, carried out experiments and analysed data in consultation with J.S.A and M.F.W. J.S.A. helped A.S. design experiments, carried out experiments and formal analysis. S.G. cloned and purified proteins. M.F.W. conceptualised the project, obtained funding, carried out formal analysis and prepared the original draft of the manuscript. All authors contributed to writing, review and editing.

FUNDING

Biotechnology and Biological Sciences Research Council [REF BB/S000313/1 to M.F.W.]; Funding for open access charge: RCUK block grant.
Conflict of interest statement. None declared.

REFERENCES

1. Samai,P., Pyenson,N., Jiang,W., Goldberg,G.W., Hatoum-Aslan,A. and Marraffini,L.A. (2015) Co-transcriptional DNA and RNA cleavage during type III CRISPR-Cas immunity. *Cell*, **161**, 1164–1174.
2. Elmore,J.R., Sheppard,N.F., Ramia,N., Deighan,T., Li,H., Terns,R.M. and Terns,M.P. (2016) Bipartite recognition of target RNAs activates DNA cleavage by the Type III-B CRISPR-Cas system. *Genes Dev.*, **30**, 447–459.
3. Estrella,M.A., Kuo,F.T. and Bailey,S. (2016) RNA-activated DNA cleavage by the Type III-B CRISPR-Cas effector complex. *Genes Dev.*, **30**, 460–470.
4. Rouillon,C., Athukoralage,J.S., Graham,S., Grüschow,S. and White,M.F. (2018) Control of cyclic oligoadenylate synthesis in a type III CRISPR system. *eLife*, **7**, e36734.
5. Niewoehner,O., Garcia-Doval,C., Rostol,J.T., Berk,C., Schwede,F., Bigler,L., Hall,J., Marraffini,L.A. and Jinek,M. (2017) Type III CRISPR-Cas systems produce cyclic oligoadenylate second messengers. *Nature*, **548**, 543–548.
6. Kazlauskiene,M., Kostiuk,G., Venclovas,C., Tamulaitis,G. and Siksnys,V. (2017) A cyclic oligonucleotide signaling pathway in type III CRISPR-Cas systems. *Science*, **357**, 605–609.
7. Nasef,M., Muffly,M.C., Beckman,A.B., Rowe,S.J., Walker,F.C., Hatoum-Aslan,A. and Dunkle,J.A. (2019) Regulation of cyclic oligoadenylate synthesis by the *S. epidermidis* Cas10-Csm complex. *RNA*, **25**, 948–962.
8. Foster,K., Kalter,J., Woodside,W., Terns,R.M. and Terns,M.P. (2019) The ribonuclease activity of Csm6 is required for anti-plasmid immunity by Type III-A CRISPR-Cas systems. *RNA Biol*, **16**, 449–460.
9. Jia,N., Jones,R., Yang,G., Ouerfelli,O. and Patel,D.J. (2019) CRISPR-Cas III-A Csm6 CARF domain is a ring nuclease triggering stepwise cA_4 Cleavage with ApA>p formation terminating RNase activity. *Mol. Cell*, **75**, 933–943.
10. Molina,R., Stella,S., Feng,M., Sofos,N., Jauniskis,V., Pozdnyakova,I., Lopez-Mendez,B., She,Q. and Montoya,G. (2019) Structure of Csx1-cOA4 complex reveals the basis of RNA decay in Type III-B CRISPR-Cas. *Nat. Commun.*, **10**, 4302.
11. McMahon,S.A., Zhu,W., Rambo,R., Graham,S., White,M.F. and T.M.,G. (2020) Structure and mechanism of a Type III CRISPR defence DNA nuclease activated by cyclic oligoadenylate. *Nat. Commun.*, **11**, 500.
12. Rostol,J.T. and Marraffini,L.A. (2019) Non-specific degradation of transcripts promotes plasmid clearance during type III-A CRISPR-Cas immunity. *Nat. Microbiol.*, **4**, 656–662.
13. Athukoralage,J.S., Graham,S., Rouillon,C., Grüschow,S., Czekster,C.M. and White,M.F. (2020) The dynamic interplay of host and viral enzymes in type III CRISPR-mediated cyclic nucleotide signalling. bioRxiv doi: https://doi.org/10.1101/2020.02.12.946046, 17 February 2020, pre-print: not peer reviewed.
14. Athukoralage,J.S., Rouillon,C., Graham,S., Grüschow,S. and White,M.F. (2018) Ring nucleases deactivate Type III CRISPR ribonucleases by degrading cyclic oligoadenylate. *Nature*, **562**, 277–280.
15. Athukoralage,J.S., Graham,S., Grüschow,S., Rouillon,C. and White,M.F. (2019) A type III CRISPR ancillary ribonuclease degrades its cyclic oligoadenylate activator. *J. Mol. Biol.*, **431**, 2894–2899.
16. Athukoralage,J.S., McMahon,S.A., Zhang,C., Gruschow,S., Graham,S., Krupovic,M., Whitaker,R.J., Gloster,T.M. and White,M.F. (2020) An anti-CRISPR viral ring nuclease subverts type III CRISPR immunity. *Nature*, **577**, 572–575.
17. Waterhouse,A., Bertoni,M., Bienert,S., Studer,G., Tauriello,G., Gumienny,R., Heer,F.T., de Beer,T.A.P., Rempfer,C., Bordoli,L. *et al.* (2018) SWISS-MODEL: homology modelling of protein structures and complexes. *Nucleic Acids Res.*, **46**, W296–W303.
18. Lapinaite,A., Doudna,J.A. and Cate,J.H.D. (2018) Programmable RNA recognition using a CRISPR-associated Argonaute. *Proc. Natl. Acad. Sci. U.S.A.*, **115**, 3368–3373.
19. Griffin,M.A., Davis,J.H. and Strobel,S.A. (2013) Bacterial toxin RelE: a highly efficient ribonuclease with exquisite substrate specificity using atypical catalytic residues. *Biochemistry*, **52**, 8633–8642.
20. Rouillon,C., Athukoralage,J.S., Graham,S., Grüschow,S. and White,M.F. (2019) Investigation of the cyclic oligoadenylate signalling pathway of type III CRISPR systems. *Methods Enzymol.*, **616**, 191–218.
21. Grüschow,S., Athukoralage,J.S., Graham,S., Hoogeboom,T. and White,M.F. (2019) Cyclic oligoadenylate signalling mediates *Mycobacterium tuberculosis* CRISPR defence. *Nucleic Acids Res.*, **47**, 9259–9270.
22. Yan,X., Guo,W. and Yuan,Y.A. (2015) Crystal structures of CRISPR-associated Csx3 reveal a manganese-dependent deadenylation exoribonuclease. *RNA Biol.*, **12**, 749–760.
23. Han,W., Pan,S., Lopez-Mendez,B., Montoya,G. and She,Q. (2017) Allosteric regulation of Csx1, a type IIIB-associated CARF domain ribonuclease by RNAs carrying a tetraadenylate tail. *Nucleic Acids Res.*, **45**, 10740–10750.
24. Lau,R.K., Ye,Q., Birkholz,E.A., Berg,K.R., Patel,L., Mathews,I.T., Watrous,J.D., Ego,K., Whiteley,A.T., Lowey,B. *et al.* (2020) Structure and mechanism of a cyclic trinucleotide-activated bacterial endonuclease mediating bacteriophage immunity. *Mol. Cell*, **77**, 723–733.
25. Ye,Q., Lau,R.K., Mathews,I.T., Birkholz,E.A., Watrous,J.D., Azimi,C.S., Pogliano,J., Jain,M. and Corbett,K.D. (2020) HORMA domain proteins and a trip13-like ATPase regulate bacterial cGAS-like enzymes to mediate bacteriophage immunity. *Mol. Cell*, **77**, 709–722.
26. Cohen,D., Melamed,S., Millman,A., Shulman,G., Oppenheimer-Shaanan,Y., Kacen,A., Doron,S., Amitai,G. and Sorek,R. (2019) Cyclic GMP-AMP signalling protects bacteria against viral infection. *Nature*, **574**, 691–695.
27. Whiteley,A.T., Eaglesham,J.B., de Oliveira Mann,C.C., Morehouse,B.R., Lowey,B., Nieminen,E.A., Danilchanka,O., King,D.S., Lee,A.S.Y., Mekalanos,J.J. *et al.* (2019) Bacterial cGAS-like enzymes synthesize diverse nucleotide signals. *Nature*, **567**, 194–199.